

# Measurement of the $^{21}\text{Ne}$ Zeeman frequency shift due to Rb- $^{21}\text{Ne}$ collisions

R. E. Stoner and R. L. Walsworth

*Harvard-Smithsonian Center for Astrophysics, Cambridge, Massachusetts 02138*

(Received 24 October 2001; published 16 September 2002)

Using a  $^{21}\text{Ne}$ - $^3\text{He}$  Zeeman maser, we compared the frequency shift of the  $^{21}\text{Ne}$  nuclear Zeeman resonance induced by polarized Rb vapor to the shift induced in the  $^3\text{He}$  nuclear Zeeman resonance. The  $^3\text{He}$ -Rb shift has recently been measured with high precision [M.V. Romalis and G.D. Cates, *Phys. Rev. A* **58**, 3004 (1998)], permitting the conversion of our differential measurement to an absolute value for the  $^{21}\text{Ne}$ -Rb shift. We report a value of  $\kappa_{21} = 32.0 \pm 2.9$  for the Rb- $^{21}\text{Ne}$  contact shift enhancement factor at a temperature of approximately 128 °C. We also propose high-precision differential contact shift measurements, the absolute accuracy of which could be limited by the error in the  $^3\text{He}$  contact shift.

DOI: 10.1103/PhysRevA.66.032704

PACS number(s): 32.80.Bx, 32.60.+i, 84.40.Ik, 34.20.-b

## I. INTRODUCTION

Polarization of noble gases by spin exchange with optically pumped alkali-metal vapors [1,2] is an important technique for a variety of scientific and technological applications. Polarized noble gases have been used for precise measurements of the neutron spin structure function [3]; neutron polarizers and analyzers [4]; magnetic resonance imaging [5–7]; studies of gas diffusion in porous media [8]; gain media for Zeeman masers [9–12]; and tests of fundamental symmetries [13–17].

Recently, Kostelecky and Lane reported that a  $^{21}\text{Ne}$ - $^3\text{He}$  differential magnetometer could be used in a precision test of Lorentz and CPT (charge conjugation, parity, and time reversal symmetries) [18]. We have proposed to develop a two-species  $^{21}\text{Ne}$ - $^3\text{He}$  Zeeman maser to carry out such a fundamental symmetry test [19].

The spin-exchange interaction between alkali and noble-gas atoms has been extensively described in the literature [2,20–25]. During spin-exchange collisions, there is significant overlap of the alkali atom's valence electron wave function with the noble-gas nucleus which comprises a Fermi contact interaction of the form

$$H_{\text{int}} = \alpha \vec{K} \cdot \vec{S}, \quad (1)$$

where  $\vec{S}$  and  $\vec{K}$  are the electron and nuclear spin angular momentum operators, respectively. This interaction leads to exchange of angular momentum between the alkali valence electron and the noble-gas nucleus. During the collision, the valence electron and nucleus experience a strong magnetic field from the close proximity of their spin magnetic moments. In spite of the small fraction of the time spent in collision, the average magnetic fields experienced by both the alkali valence electron and the noble-gas nucleus can be affected if either the alkali or noble-gas species is polarized. The resultant change in the Larmor precession frequency for either species, referred to as the contact shift, is expressed in terms of an enhancement factor,  $\kappa$ , which is defined for collocated spherical distributions of the alkali and noble-gas magnetizations. For each species,  $\kappa$  is the ratio of the total Larmor frequency shift, induced both by the contact interaction and by the classical magnetic field generated by the other

species' magnetization, to the shift induced by the classical magnetization alone.  $\kappa$  can be much greater than unity, growing with increasing  $Z$  of the noble-gas nucleus [23]. In the limit where the formation of alkali-noble-gas van der Waals molecules is a negligible part of the spin-exchange interaction (true for the experiment reported in this paper), a single enhancement factor describes the contact shift of the noble-gas Zeeman splitting by the alkali atoms, and vice versa [22]. The frequency shift experienced by noble-gas atoms in the presence of polarized alkali atoms, including both the contact shift and the shift due to classical magnetization fields, is

$$\delta\omega_{\text{ng}} = (\kappa - 1 + f_{\text{DDF}}) \gamma_{\text{ng}} \frac{8\pi}{3} g_S \mu_B [a] \langle S_z \rangle / \hbar. \quad (2)$$

Recall the elementary result that  $(8\pi/3)M$  is the magnetic-field strength inside a magnetized sphere with magnetic dipole moment density (i.e., magnetization)  $M$ ; the field is uniform and parallel to the magnetization.  $f_{\text{DDF}}$  is a dimensionless factor that accounts for the effect of classical magnetization fields ("distant dipole fields" [25]), and is unity for a spherical distribution of magnetization.  $[a]$  is the number per unit volume of alkali atoms, and  $\gamma_{\text{ng}}$  is the gyromagnetic ratio of the noble-gas species. For convenience, we define the component of alkali atom magnetization along the magnetic field ( $z$ ) axis,  $M_a$ , as

$$M_a = g_S \mu_B [a] \langle S_z \rangle / \hbar. \quad (3)$$

The alkali nuclear magnetic moments do not contribute to the contact shift, but do weakly affect the distant dipole fields produced by the alkali magnetization distribution. We ignored these nuclear contributions to the distant dipole fields, since they were too small to bear on the results reported in this work.

In precision measurements it is important to be able to monitor the absolute polarization of the noble gases. Romalis and Cates [25] demonstrated accurate polarimetry of  $^3\text{He}$  using the Rb Zeeman frequency shift due to Rb- $^3\text{He}$  spin exchange collisions, and made a very precise measurement of the Rb- $^3\text{He}$  enhancement factor. Future use of  $^{21}\text{Ne}$  in precision measurement applications would benefit from contact shift polarimetry, but there is to date no published mea-

surement of the Rb- $^{21}\text{Ne}$  enhancement factor. In this paper, we present the first such measurement. We measured the net Larmor frequency shifts, simultaneously impressed by the presence of polarized Rb, on ensembles of polarized  $^3\text{He}$  and  $^{21}\text{Ne}$  precessing in the same (nearly) spherical glass cell. The measurement presented in this paper is not the first in which a ratio of contact shift enhancement factors was determined. Baranga *et al.* measured the shifts of the Larmor precession frequencies of Rb and K vapors residing in the same cell, induced simultaneously by the presence of polarized  $^3\text{He}$  [24].

The experiment is described in Sec. II. Determining the ratio of the Rb-induced shifts permitted us to divide out the dependence on Rb magnetization, and express the  $^{21}\text{Ne}$  enhancement factor  $\kappa_{21}$  in terms of the  $^3\text{He}$  enhancement factor  $\kappa_3$ . Using the very accurate measurement of  $\kappa_3$  by Romalis and Cates, we determined the absolute contact shift enhancement factor  $\kappa_{21}$ . Analysis of the data is presented in Sec. III. Suggestions for improved measurements are given in Sec. IV.

## II. APPARATUS, PROCEDURE, SYSTEM PARAMETERS

We employed a two-species  $^{21}\text{Ne}$ - $^3\text{He}$  Zeeman maser to establish simultaneous stable precession of the  $^{21}\text{Ne}$  and  $^3\text{He}$  ensembles in the same sealed glass cell. The  $^{21}\text{Ne}$ - $^3\text{He}$  maser is a new device that will be described elsewhere; that description is summarized here. Figure 1 is a schematic representation of the maser. Circularly polarized light resonant with the Rb D1 transition (795 nm) was generated by a 30 W laser diode array (LDA). The light fully illuminated a 1.4-cm-diam (near-)spherical sealed glass cell containing (at room temperature) 228 torr of  $^{21}\text{Ne}$ , 266 torr of  $^3\text{He}$ , 31 torr of  $\text{N}_2$ , and Rb metal of natural isotopic composition [26]. The LDA light propagated along the axis of a uniform magnetic field of strength 3 G. The field was generated by a precision solenoid/ $\mu$ -metal-shield system capable of producing a 3 G magnetic field with  $\leq 35 \mu\text{G}/\text{cm}$  magnetic-field gradients, with no gradient shimming. The solenoid was driven using a current source capable of  $\sim 3$  ppm stability over time scales of order 1000 s. The glass cell was heated both by the LDA light and blown hot air to a temperature of approximately 125 °C (see Sec. III). The temperature of the air surrounding the cell was controlled to about 43 mK, as measured by a three-lead nonmagnetic platinum resistance thermometer (known as an RTD). The total output power of the LDA was actively controlled to about a part in  $10^4$ .

The Rb vapor was polarized by optical pumping; the resulting Rb electron spin polarization was very close to unity. Even though the 30 W LDA had a very broad ( $\sim 1.5$  nm) linewidth, the on-resonant optical power was roughly 0.5 W. Thus, the optical pumping rate was  $> 10^5$  photon absorptions per second per Rb atom [27]. For the  $^{21}\text{Ne}$ ,  $^3\text{He}$ , and  $\text{N}_2$  gas pressures used in the present experiment, the rate of Rb polarization destruction events per Rb atom is  $< 10^3 \text{ s}^{-1}$  [2]. We thus conclude that the volume-averaged Rb electron spin polarization was greater than 0.99 during the frequency shift experiment. Pickup coils wound in series were placed in close proximity to the cell. The coils were excited by the

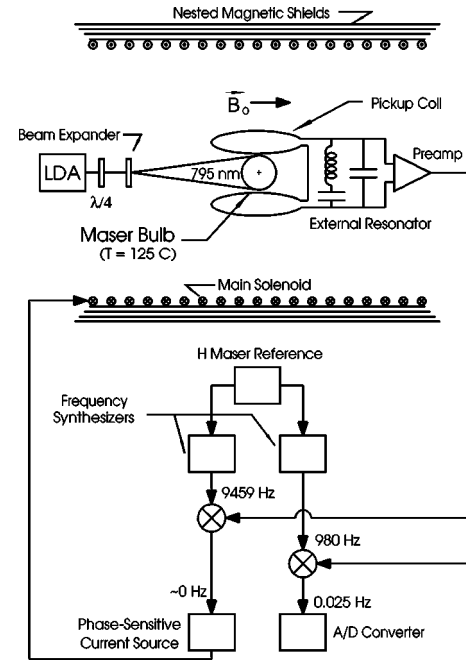


FIG. 1. Schematic of the two-species  $^{21}\text{Ne}$ - $^3\text{He}$  Zeeman maser. The device operates similarly to the  $^{129}\text{Xe}$ - $^3\text{He}$  maser [10,11], except that the  $^{21}\text{Ne}$ - $^3\text{He}$  maser employs a single- rather than a double-bulb cell. Colocated ensembles of noble-gas atoms are polarized by spin-exchange collisions with optically pumped Rb atoms. Precession of polarized atoms excites current in nearby inductive pickup coils, which are part of a circuit tuned with resonances near the Larmor precession frequencies of the two noble-gas species. The current induces magnetic fields which act back on the precessing atoms, providing feedback for maser oscillation.

magnetic flux associated with the precession of the polarized noble gases. The coils were part of a tuned circuit with resonances at both noble-gas precession frequencies:  $\approx 9459$  Hz for  $^3\text{He}$  and 980 Hz for  $^{21}\text{Ne}$ . The large current flow induced in the pickup coils by resonant excitation resulted in magnetic fields oscillating at the noble-gas nuclear Larmor frequencies being impressed back on the precessing atoms. This feedback resulted in steady-state maser operation for both species. The maser amplitudes were not affected by small changes in the LDA output power, which again indicates that the volume-averaged Rb electron-spin polarization was very close to unity.

$^{21}\text{Ne}$  has nuclear spin 3/2, and thus a quadrupole moment. The quadrupole moments of the  $^{21}\text{Ne}$  ensemble interacted coherently with electric-field gradients at the glass cell walls, shifting the four Zeeman energy levels so as to split the three (otherwise degenerate) dipole transitions [28]. The splitting ( $\delta\omega_Q$ ) is proportional to  $3 \cos^2 \theta - 1$ , where  $\theta$  is the angle of the cell's cylindrical symmetry axis (defined by the cell's small pull-off stem) with the magnetic field. We oriented the cell as close as possible to the "magic angle"  $\cos \theta = \sqrt{1/3}$  to minimize the quadrupole splitting. Remnant quadrupole wall shifts in the cell were not measured; however, computer simulations indicate that without proper cell orientation, realistic-sized splittings can disrupt  $^{21}\text{Ne}$  maser oscillation. Nevertheless, we found it was straightforward to attain  $^{21}\text{Ne}$

maser oscillation with a steady-state amplitude. We observed a small ( $\sim 10 \mu\text{Hz}$ ) sinusoidal modulation of the  $^{21}\text{Ne}$  maser frequency, with a period of about 16 h. We speculate that the modulation was a consequence of a remnant quadrupole splitting resulting from cell orientation error. The effect was small, with a period much longer than the duration of our frequency shift measurements, and thus was not a source of significant systematic error.

The  $^3\text{He}$  and  $^{21}\text{Ne}$  maser signals were presented to a low-noise preamplifier. The preamp output was then analyzed using lock-in amplifiers, which were referenced to a set of synchronized signal generators tuned near the noble-gas maser frequencies and locked to a hydrogen-maser-derived 5 MHz signal. The phases of both noble-gas maser signals were recorded digitally at a sample rate of 1 Hz. The analog-to-digital sampling trigger was also derived from the master 5 MHz reference.

The experiment consisted of observing the maser phases during a series of reversals of the direction of the Rb polarization. We reversed the Rb polarization about every 140 s by rotation of the quarter-wave plates used for circular polarization of the optical pumping light (Fig. 1). We typically achieved Rb polarization reversals in  $\leq 20$  s. The total duration of a set of reversals was about 1000 s, limited by magnetic-field stability as well as the extent to which the noble-gas masers' steady states were disrupted by the alternating Rb polarization. We acquired two sets of reversal data. Clear changes in the slopes of the noble-gas maser phase curves were precisely correlated with reversal of the Rb polarization direction; these frequency changes were the result of the contact shift combined with the (classical) shift due to the Rb magnetization distribution. The change of noble-gas maser oscillation frequency induced by Rb polarization reversal was about 44 mHz for the  $^{21}\text{Ne}$  maser and 71 mHz for the  $^3\text{He}$  maser.

### III. DATA AND ANALYSIS

Phase data for the second of the two measurement scans are shown in Figs. 2 and 3. We model the  $^{21}\text{Ne}$  phase  $\varphi_{21}$  (see Fig. 2) and the  $^3\text{He}$  phase  $\varphi_3$  (see Fig. 3) acquired by the lock-in amplifiers as evolving according to the following equations:

$$\begin{aligned} \varphi_{21} &= \varphi_{21,o} + \gamma_{21} B_o t - 2\pi\nu_{\text{ref},21} + \gamma_{21} \int_0^t dt' \delta B(t') \\ &\quad + (\kappa_{21} - 1 + f_{\text{DDF}}) \gamma_{21} \frac{8\pi}{3} \int_0^t dt' M_{\text{Rb}}(t'), \\ \varphi_3 &= \varphi_{3,o} + \gamma_3 B_o t - 2\pi\nu_{\text{ref},3} + \gamma_3 \int_0^t dt' \delta B(t') \\ &\quad + (\kappa_3 - 1 + f_{\text{DDF}}) \gamma_3 \frac{8\pi}{3} \int_0^t dt' M_{\text{Rb}}(t'), \end{aligned} \quad (4)$$

where  $\gamma_{21}$  ( $\gamma_3$ ) is the gyromagnetic ratio of  $^{21}\text{Ne}$  ( $^3\text{He}$ );  $\kappa_{21}$  ( $\kappa_3$ ) is the enhancement factor for  $^{21}\text{Ne}$  ( $^3\text{He}$ );  $f_{\text{DDF}}$  is the dimensionless factor to account for the classical magnetic

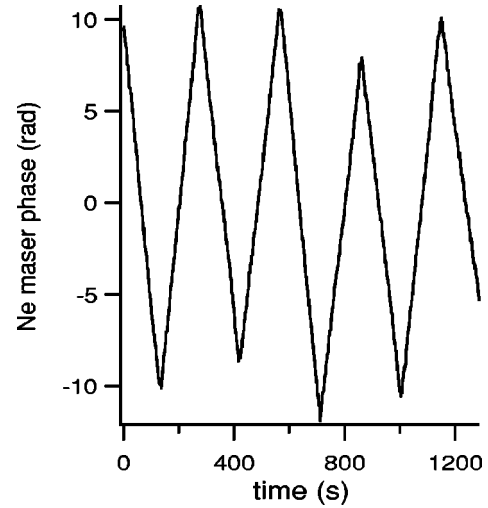


FIG. 2.  $^{21}\text{Ne}$  maser phase profile from one (of two) measurement scans. Phase dependence linear in time has been removed.

field due to the Rb magnetization;  $\nu_{\text{ref},21}$  and  $\nu_{\text{ref},3}$  are the reference frequencies presented to the lock-in amplifiers;  $B_o$  is the time-average magnetic-field strength over the time interval;  $\delta B$  is the time-dependent deviation of the magnetic field from its mean value; and  $M_{\text{Rb}}$  is the Rb magnetization. Note that independent maser frequency measurements determined the ratio of the two gyromagnetic ratios,  $\gamma_3/\gamma_{21}$ , to an accuracy much better than 1 ppm. Also, the effects on the maser phases of magnetic fields due to noble-gas magnetization have been neglected in comparison to the contact shift and Rb magnetization effects; this assumption is reasonable for the noble-gas magnetizations and relatively rapid Rb polarization reversals of the present experiment (see below).

Magnetic-field drift occurred over the course of the measurement scan. However, the  $^{21}\text{Ne}$  and  $^3\text{He}$  masers are colocated magnetometers, so that we can construct a data set

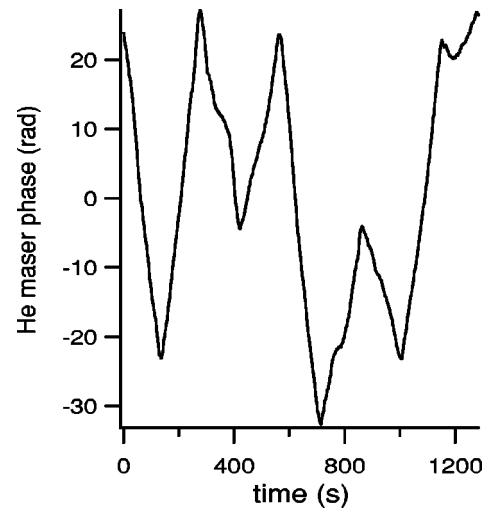


FIG. 3.  $^3\text{He}$  maser phase profile measured simultaneously with the data of Fig. 2. Phase dependences linear in time have been removed. Note the considerable distortion in this phase curve due to magnetic-field drift.

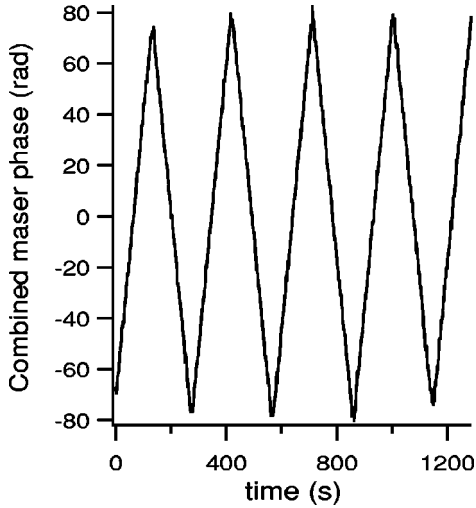


FIG. 4. The combined phase  $\Delta\varphi$  of the two masers as per Eq. (5) for the measurements of Figs. 2 and 3. This profile is proportional to the phase variation induced by the Rb–noble-gas contact shift alone. The sawtooth shape arises from periodic reversal of the Rb polarization, which reverses the Rb–noble-gas contact frequency shift. The highly regular shape of the difference curve reflects the fact that magnetic-field drift effects are subtracted out.

from which the effects of magnetic-field drift and Rb distant dipole fields have been removed. We define

$$\Delta\varphi \equiv \varphi_3 - \frac{\gamma_3}{\gamma_{21}}\varphi_{21}. \quad (5)$$

It is easily shown that

$$\Delta\varphi = \varphi_{3,o} - \varphi_{21,o} + 2\pi \left( \frac{\gamma_3}{\gamma_{21}} \nu_{\text{ref},21} - \nu_{\text{ref},3} \right) t + (\kappa_3 - \kappa_{21}) \gamma_3 \frac{8\pi}{3} \int_0^t dt' M_{\text{Rb}}(t'). \quad (6)$$

Aside from a trivial phase offset and known linear phase evolution,  $\Delta\varphi$  reflects the action of the Rb contact shifts only: phase evolution due to magnetic fields is subtracted off. This combined phase profile is plotted in Fig. 4. As seen in this figure, the phase evolution due to the contact shift was a piecewise-linear “sawtooth” profile, which is just the time integral of the square-wave modulation of the maser frequencies induced by the Rb polarization reversals. Since our measurement is derived from computing the differences in slopes between adjacent linear regions of the phase curve, removal of constant and linear dependence from the phase data had no effect on the result. Thus, our plots of the phase data shown in Figs. 2, 3, and 4 are displayed with a mean value and mean slope of zero.

If the Rb magnetization were known, one could immediately deduce  $\kappa_{21}$  using Eq. (6) and the value of  $\kappa_3$  from [25]. Even though the Rb electron spin polarization was very close to unity, the Rb density was not known *a priori*. It was therefore necessary to consider the ratio of contact shifts impressed on the  $\varphi_{21}$  and the  $\Delta\varphi$  phase curves, and then deter-

mine the Rb density self-consistently. (The contact shifts also have a weak temperature dependence [25] which must be taken into account.)

We analyzed the data in two ways, which yielded essentially identical results. First, we computed the average changes in slope of the phase curves  $\varphi_{21}$  and  $\Delta\varphi$  caused by the reversals of the Rb magnetization. That is, we used a least-squares linear fitting routine to extract the slope of each piecewise linear region of the phase curves. We then recorded the differences in slope of adjacent regions for each of the phase curves, and computed mean absolute values of the slope differences for each data set defined as  $M_{21}$  and  $\Delta M$  for the  $\varphi_{21}$  and  $\Delta\varphi$  profiles, respectively. We estimated uncertainties from the standard deviation of the mean in the slope differences’ absolute values.

We define the ratio of mean slope changes as  $\mathcal{R} \equiv M_{21}/\Delta M$ . The weighted average value for  $\mathcal{R}$  from the two data sets was  $\mathcal{R} = 0.1262 \pm 0.0025$ , where a one-sigma uncertainty is reported. The uncertainty was almost entirely due to that in  $M_{21}$ . The fractional uncertainty in  $\Delta M$  for both of the data sets was  $< 0.1\%$ , which indicates that Rb polarization reversal was achieved to high precision and that the Rb magnetization was stable to better than 0.1% over the course of the measurements. The fractional uncertainty in  $M_{21}$  was much larger,  $\sim 2\%$ , because of magnetic-field drift. In principle, we could have analyzed the  $\varphi_3$  profile rather than  $\varphi_{21}$ , but magnetic-field drift effects were  $\gamma_3/\gamma_{21} = 9.65$  times larger for  $\varphi_3$  than  $\varphi_{21}$ , making it impractical to extract slope data from  $\varphi_3$  directly (see Fig. 3).

We found it was *not* necessary to account for variations in maser frequency due to changes in noble-gas longitudinal polarization. The magnetization of the noble gases created magnetic fields which varied in time during the course of each of the two measurement scans, as evidenced by (small) maser amplitude changes observed during the scans. A given maser’s magnetization field could not affect its own frequency, since magnetization fields were parallel to the magnetization in the near-spherical cell. However, each maser’s frequency was shifted by the other’s magnetization, and such shifts did not subtract out of  $\Delta\varphi$  as did external magnetic-field drift. The noble-gas longitudinal polarizations underwent both slow drift and periodic variations, the latter caused by the Rb polarization reversals. However, the small uncertainty in the  $\Delta\varphi$  slope differences shows that frequency variations due to slow drift in the noble-gas magnetizations had a negligible effect. We also determined that variations of the noble-gas longitudinal polarizations caused by the periodic Rb polarization reversal had a negligible effect on the contact shift measurement. Employing a Bloch equation model of Zeeman maser dynamics [9], we found that periodic reversal (i.e., square-wave modulation) of the Rb polarization induced a symmetric sawtooth-wave (i.e., integrated square-wave) modulation on the noble-gas longitudinal polarizations with peak-to-peak amplitude given approximately by  $\gamma_{\text{se}}\tau$ , where  $\gamma_{\text{se}}$  is the Rb–noble-gas spin exchange rate per noble-gas atom, provided that two conditions were satisfied for  $\tau$ , the time between Rb polarization reversals. These two conditions were  $\tau \ll (\gamma_{\text{se}} + 1/T_1)^{-1}$  and  $\tau \ll \sqrt{\tau_{\text{rd}}/2\gamma_{\text{se}}}$ , where  $T_1$  is the relaxation time for noble-gas longitudinal

polarization and  $\tau_{\text{rd}}$  is the noble-gas ensemble radiation damping time. The two conditions, which ensured that the masers were always in the regime of perturbative linear dynamics, were easily met in the present experiment, where  $\tau \approx 140$  s,  $\gamma_{\text{se}} \approx 3.2 \times 10^{-6} \text{ s}^{-1}$  for  $^3\text{He}$  and  $1.3 \times 10^{-5} \text{ s}^{-1}$  for  $^{21}\text{Ne}$  (assuming  $[\text{Rb}] \approx 2.7 \times 10^{13} \text{ cm}^{-3}$  at a temperature  $\approx 125^\circ\text{C}$ ),  $T_1 \approx 20\,000$  s for  $^3\text{He}$  and 9000 s for  $^{21}\text{Ne}$ , and  $\tau_{\text{rd}} \approx 20$  s for  $^3\text{He}$  and 500 s for  $^{21}\text{Ne}$ . The sawtooth-modulated noble-gas polarizations induced changes in the maser frequencies of approximately 2.8 mHz for the  $^3\text{He}$  maser and 0.7 mHz for the  $^{21}\text{Ne}$  maser over a typical time interval  $\tau \approx 140$  s between Rb polarization reversals. However, to the degree that  $\tau$  was constant during a measurement run, the *average* maser frequency shifts did not change from one interval to the next; thus the shifts subtracted out in the calculation of the interval-to-interval frequency changes  $M_{21}$  and  $\Delta M$  with better than 5% accuracy. We conclude that noble-gas polarization-induced magnetic fields had an insignificant systematic effect on the determination of  $\mathcal{R}$ .

It is easy to show from Eqs. (4) and (6) that the ratio  $\mathcal{R}$  can be interpreted as

$$\mathcal{R} = \left| \frac{\gamma_{21} \kappa_{21} + (f_{\text{DDF}} - 1)}{\gamma_3 \kappa_3 - \kappa_{21}} \right|, \quad (7)$$

where it is seen that the dependence on the Rb magnetization divided out. We can then use the value and estimated uncertainty for  $\mathcal{R}$  to compute the desired  $^{21}\text{Ne}$  contact shift enhancement factor  $\kappa_{21}$  at a specified noble-gas/Rb vapor temperature, once we account for the effect of classical magnetization fields created by the Rb vapor.

We now consider the second method of analyzing the data to obtain a value for  $\mathcal{R}$  and hence  $\kappa_{21}$ , which yielded essentially the same results as the above approach. While this second method is slightly more complex, it is useful because it provides a framework for estimating the size of magnetic-field drift in the present measurement. In the second method, we consider the phase data sets to be  $N$ -component vectors (denoted by a tilde), where  $N \equiv$  number of data in the set ( $\sim 10^3$  for each of the two scans). We use the  $\Delta\tilde{\varphi}$  profile as a model of the shape of the Rb magnetization-induced phase [see Eq. (6)]. We then seek to describe the  $\tilde{\varphi}_{21}$  profile vector as a linear combination of elements of a partial basis of orthonormal vectors. The partial basis includes an element corresponding to the (normalized)  $\Delta\tilde{\varphi}$  profile ( $\equiv \tilde{V}_0$ ). Additional orthogonal basis vectors  $\{\tilde{V}_i\}_{i=1, N_b-1}$  are derived from  $\Delta\tilde{\varphi}$  and Legendre polynomials  $\{P_i\}_{i=0, N_b-1}$  using Gram-Schmidt orthogonalization [30]. The number of basis vectors  $N_b$  was typically of order 10, whereas the dimension of the vector space  $N$  was of order  $10^3$ , so  $N_b \ll N$ , and we find

$$\tilde{\varphi}_{21} = \sum_{i=0}^{N_b-1} a_i \tilde{V}_i. \quad (8)$$

The coefficient of  $\tilde{V}_0$  in this linear combination,  $a_0$ , is proportional to the value for  $\mathcal{R}$  obtained from a particular data set. We determined the coefficients  $a_i$  of the linear combina-

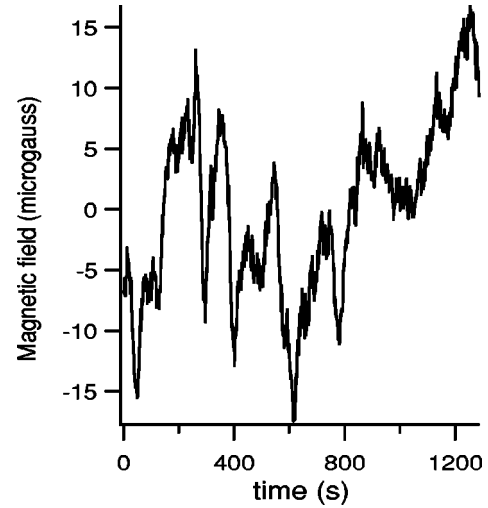


FIG. 5. Magnetic-field drift during the measurements of Figs. 2 and 3, computed from Eq. (9). The nominal field strength was 3 G, so that the fractional RMS stability of the magnetic field was about 3 ppm. Field drift was the dominant source of experimental error.

tion using both linear least-squares fitting and simple projection of  $\tilde{\varphi}_{21}$  onto the vectors of the partial basis, with identical results. We varied the number of elements in the basis set, but the coefficients obtained from the least-squares fit remained the same regardless of the size of the basis set.

Using this second data analysis method, we determined two values for  $\mathcal{R}$ , one from each data set. It was not possible to estimate uncertainties for the individual values of  $\mathcal{R}$  from the vector analysis method. Uncertainty estimates from the least-squares fit were unrealistically small because the vector analysis could not account for the effect of a nonzero projection of the magnetic-field drifts along the Rb magnetization-induced phase profile vectors. Therefore, we take the value of  $\mathcal{R}$  to be the mean of the results for the two data sets, and we coarsely estimate the uncertainty of  $\mathcal{R}$  as the deviation of the two values, to obtain  $\mathcal{R} = 0.1287 \pm 0.0036$ . This result agrees well with that of the first method of data analysis. For computing  $\kappa_{21}$  below we will use the result from the first method of analysis since the error estimate is probably more reliable.

We can compute the magnetic-field drift profile by subtracting from  $\tilde{\varphi}_{21}$  its projection on the Rb magnetization basis profile  $\tilde{V}_0$ :

$$\overline{\delta B} = \frac{1}{\gamma_{21}} \frac{d}{dt} [\tilde{\varphi}_{21} - (\tilde{\varphi}_{21} \cdot \tilde{V}_0) \tilde{V}_0]. \quad (9)$$

Note that the profile  $\overline{\delta B}$  is the magnetic field drift *orthogonal* to  $\tilde{V}_0$ . The drift profile from the second data set is plotted in Fig. 5; the time derivative of the (discretely sampled) profile was estimated by finite difference. Note that the field was stable to about  $\pm 3$  ppm RMS.

Having obtained a value for  $\mathcal{R}$ , we can then solve Eq. (7) for  $\kappa_{21}$  in terms of measured parameters, since  $\kappa_3$  is known [25]. However,  $\kappa_{21}$  is expected to be weakly temperature-dependent [23,25] and so the temperature at which the ex-

periment was carried out must be reported along with the value of  $\kappa_{21}$ . The Rb and noble-gas temperature was not reliably represented by the blown hot air temperature because the cell was also heated by the LDA. Thus, it was necessary to deduce the temperature of the noble gas and Rb vapor from the contact shift data and the known  $^3\text{He}$  enhancement factor (with its known temperature dependence). We begin by noting that the mean slope change  $\Delta M$  is related to the enhancement factors and the Rb magnetization via

$$\Delta M = 2\gamma_3 \frac{8\pi}{3} |(\kappa_3 - \kappa_{21})M_{\text{Rb}}(T)|, \quad (10)$$

where  $|M_{\text{Rb}}(T)|$  [see Eq. (3) above] is a known function of temperature. The Rb number density in  $\text{cm}^{-3}$  [Rb] is related to the temperature in kelvin of the coldest part of the cell by [29]

$$[\text{Rb}] = \frac{10^{9.318 - (4040/T)}}{(1.38 \times 10^{-17})T}. \quad (11)$$

The measured temperature dependence of the  $^3\text{He}$  enhancement factor is [25]

$$\kappa_3 = 4.52 + 0.00934T, \quad (12)$$

where  $T$  refers to the gas temperature in degrees centigrade (determined by careful cell temperature measurements in [25]). Substituting Eqs. (11) and (3) into Eq. (10) and equating all temperatures yields an equation relating  $\kappa_{21}$  and temperature (and known/measured parameters). Substituting Eq. (12) into Eq. (7) yields another equation relating  $\kappa_{21}$  and temperature. This system of two (nonlinear) equations and two unknowns can be solved to yield the temperature and  $\kappa_{21}$ . The temperature determination depends strongly on the enhancement factor, while the enhancement factor determination depends only weakly on the temperature (via the known temperature dependence of  $\kappa_3$ ). Thus, an iterative method to compute the temperature rapidly converges: an initial guess for the temperature enables calculation of  $\kappa_{21}$ , which in turn permits calculation of the Rb magnetization and hence the temperature. This corrected temperature is used to recompute a better estimate for  $\kappa_{21}$ , which is used to recompute a better estimate of the Rb magnetization, etc.

Note that the above iterative procedure yields a temperature that lies between the temperature of the coldest part of the cell (which determines [Rb] and  $M_{\text{Rb}}$ ) and the noble-gas/Rb vapor temperature (which determines  $\kappa_3$ ). Measurements in our laboratory have shown typical temperature variations of less than  $5^\circ\text{C}$  along the surface of small glass cells in conditions similar to the present experiment. In addition, recent measurements by Walter *et al.* [31] have quantified the elevation of the gas temperature above the cell wall temperature due to absorption of pumping light. In our system, less than 1 W of LDA light was absorbed by the Rb vapor, implying from [31] an elevation of  $\sim 1^\circ\text{C}$  in the noble-gas/Rb vapor temperature. Therefore, accounting for both the typical temperature variation on the glass cell wall

and the elevated temperature of the gas, we correct the temperature given by the iterative method from  $(124.8 \pm 1.9)^\circ\text{C}$  to  $(128 \pm 3)^\circ\text{C}$ .

Using the result  $\mathcal{R} = 0.1262 \pm 0.0025$  from the slope difference analysis, taking  $f_{\text{DDF}} = 1$  (see the justification below), and including the effect of the above small temperature correction, we determine the contact shift enhancement factor for Rb and  $^{21}\text{Ne}$  to be  $\kappa_{21} = 32.0 \pm 2.9$  at a temperature of  $(128 \pm 3)^\circ\text{C}$ . We are not aware of a previous measurement of the Rb- $^{21}\text{Ne}$  contact shift. Walker estimated the Rb- $^{21}\text{Ne}$  enhancement factor to be 38 at a similar temperature, and the ratio of the Rb- $^{21}\text{Ne}$  and Rb- $^3\text{He}$  enhancement factors to be 4.3 [23]. We report this ratio to be  $5.6 \pm 0.5$ .

The 3% uncertainty in  $\mathcal{R}$  dominates other sources of error, inducing a 9% uncertainty in  $\kappa_{21}$ . The 1.5% uncertainty in the  $^3\text{He}$  enhancement factor  $\kappa_3$  contributed to a 0.8% uncertainty in  $\kappa_{21}$ . The uncertainty in temperature induced a 0.5% uncertainty in  $\kappa_{21}$ . To the extent that the cell could be described as an ellipsoid of revolution, then departure from a spherical Rb magnetization distribution induced an uncertainty of 0.15% in  $\kappa_{21}$  with zero systematic correction. (The glass cell's "pull-off" volume was very small,  $\sim 10\text{ mm}^3$ , and so contributed negligibly to the Rb magnetization distribution.)

The claim of zero systematic correction of the classical magnetization field shift for an ellipsoidal cell is justified by noting that (i) the classical magnetization field inside an ellipsoid of uniform magnetization is uniform, with its magnitude depending on the ellipsoid's dimensions and the relative orientation of the ellipsoid major axis and the magnetization vector; and (ii) when the ellipsoid major axis is oriented at the magic angle  $\theta_m = \cos^{-1}(1/\sqrt{3})$  with respect to the magnetization direction, the component of the classical magnetization field parallel to the magnetization is exactly that of a spherical distribution with the same magnetization, regardless of the ellipsoid's dimensions. We oriented the cell at  $\theta_m$  in order to suppress  $^{21}\text{Ne}$  quadrupole wall shifts, with an uncertainty of about  $10^\circ$ . The  $10^\circ$  uncertainty in orientation leads to the estimated uncertainty of 0.15% in  $\kappa_{21}$  due to the measured asphericity of the cell.

#### IV. SUGGESTIONS FOR IMPROVED MEASUREMENTS; CONCLUSIONS

There are straightforward improvements that could be implemented to reduce the uncertainty in the present measurement. The experiment was conducted in the course of developing a  $^{21}\text{Ne}$ - $^3\text{He}$  dual Zeeman maser, so that opportunities for taking contact shift data were very limited. A factor of 3 improvement in the result could easily be achieved just by taking ten times more data. Active magnetic-field stabilization using an independent magnetometer [25] would essentially eliminate field drift, reducing statistical uncertainty in the measurement to that due to phase noise, a factor of  $> 0.03/0.001 = 30$  reduction. Active field stabilization would also permit a reduction in the phase noise since the signal acquisition bandwidth could be reduced by at least a factor of 3, so that the statistical uncertainty could be reduced by about a factor of 300 compared to the present experiment.

This uncertainty would already be less than that contributed by cell asphericity (0.15%) and uncertainty in temperature (0.5%). Thus, the absolute uncertainty in the Rb- $^{21}\text{Ne}$  contact shift enhancement factor  $\kappa_{21}$  would be limited by the 1.5% uncertainty in  $\kappa_3$ , whereas the ratio  $\kappa_{21}/\kappa_3$  would be known to an uncertainty of only a few tenths of one percent.

It may be possible to measure ratios of alkali–noble-gas enhancement factors to a level below a part in  $10^3$  if one could eliminate effects of the classical magnetization field shift. We have already shown that one can use differential magnetometry to obtain data from which classical magnetization field shifts are eliminated to high precision. We suggest here that with a three-species noble-gas maser one could measure the contact shift enhancement factor of a third species if the other two species' enhancement factors are known, *independent of the classical magnetization field shift*. Even though it has not yet been done, we believe it is a straightforward matter to implement a three-species maser in a single-bulb glass cell.

A comprehensive set of contact shift data would serve as a probe of noble-gas–alkali interaction potentials [23]. A program using multispecies noble-gas masers to measure contact shift ratios could be implemented using  $^{129}\text{Xe}$ ,  $^{83}\text{Kr}$ ,  $^{21}\text{Ne}$ , and  $^3\text{He}$  along with K, Cs, and Rb in turn. Contact shift ratios would be converted to absolute values for enhancement factors by using the measured values for  $^3\text{He}/\text{Rb}$  [25] and  $^3\text{He}/\text{K}$  [24]. (The enhancement factor for  $^3\text{He}/\text{Cs}$  has not yet been measured.) Na would be a poor candidate for use in a noble-gas maser because of its relatively low vapor pressure. The remaining stable noble-gas isotope with nonzero nuclear spin,  $^{131}\text{Xe}$ , cannot be used with the other noble gases in a multispecies maser because its nuclear dipole moment has a sign opposite to that of the others (making it impossible to achieve a population inversion simultaneously with the other species). However, it may be possible to measure the  $^{131}\text{Xe}$  precession frequency in free induction decay in the presence of two other noble-gas masers.

Measuring contact shift ratios precisely could proceed as follows: one would first measure the ratio of the enhancement factors of  $^{83}\text{Kr}$  and  $^{129}\text{Xe}$  to each other. The contact shift enhancement factors for  $^{83}\text{Kr}$  and  $^{129}\text{Xe}$  are estimated by Walker to be about 230 and 730, respectively [23]. Using an independent magnetometer with the colocated Xe-Kr masers, it may be possible to measure the ratio of the (large) enhancement factors of Xe and Kr to below a part in  $10^3$  even if the classical magnetization field were accounted for

only to the 10% level. (An accounting of  $\sim 1\%$  is claimed in the present work.) Triple masers using  $^{83}\text{Kr}$  and  $^{129}\text{Xe}$ , along with  $^{21}\text{Ne}$  and  $^3\text{He}$  in turn, would yield high-precision measurements of the ratios of all the enhancement factors; the known enhancement factor for  $^3\text{He}$  would then determine the absolute values of the other enhancement factors. Temperature dependences could of course also be measured. In particular, enhancement factor ratios as a function of density (normalized to some experimental reference density) could be determined to very high precision. Improved cell thermometry could eliminate the need to depend on a temperature-density calibration [29] to determine the cell temperature. Measurements as a function of optical pumping laser power could allow for an accounting of the effects of absorptive gas heating.

We see two significant technical challenges to the suggested three-species maser scheme. First, for very-high-precision measurements, control of the noble-gas magnetization fields would need to be maintained more carefully than in the present work. A possible solution would be to decrease the time between polarization reversals in order to increase the relative size of the contact shifts in comparison to noble-gas polarization-induced frequency shifts. The second challenge is the need to account carefully for the contribution of van der Waals molecule formation to the contact frequency shifts, particularly for the more polarizable  $^{83}\text{Kr}$  and  $^{129}\text{Xe}$  species [2]. We estimate that absolute pressure measurements accurate to a few percent for each species will be required to determine contact shift enhancement factors to better than a part in  $10^3$ . It may also be necessary to make contact shift measurements as a function of the partial pressure of each constituent gas. (Such measurements might in turn provide useful information about the formation and break-up of noble-gas van der Waals molecules.)

Finally, we remark that a two-species maser using  $^3\text{He}$  and  $^{21}\text{Ne}$  has been proposed for a high-precision test of CPT and Lorentz symmetry [19]. In such a device, Rb–noble-gas contact shifts would be an important systematic effect. However, adding a colocated  $^{129}\text{Xe}$  maser could provide a high-precision *in situ* measurement of the Rb magnetization, potentially rendering this systematic effect negligible.

#### ACKNOWLEDGMENTS

We thank T. Chupp for the use of the  $^{21}\text{Ne}$ - $^3\text{He}$  cell, and gratefully acknowledge D. Phillips and D. Bear for helpful conversations.

- 
- [1] M.A. Bouchiat, T.R. Carver, and C.M. Varnum, *Phys. Rev. Lett.* **5**, 373 (1960).  
 [2] T. Walker and W. Happer, *Rev. Mod. Phys.* **69**, 629 (1997).  
 [3] K. Abe *et al.*, *Phys. Rev. Lett.* **79**, 26 (1997); *Phys. Lett. B* **404**, 377 (1997).  
 [4] G.L. Greene, A.K. Thompson, and M.S. Dewey, *Nucl. Instrum. Methods Phys. Res. A* **356**, 177 (1995).  
 [5] M.S. Albert, G.D. Cates, B. Driehuys, W. Happer, B. Saam, C.S. Springer, Jr., and A. Wishnia, *Nature (London)* **370**, 199

- (1994); H. Middleton, L.W. Hedlund, G.A. Johnson, K. Juvan, and J. Schwartz, *Magn. Reson. Med.* **33**, 271 (1995).  
 [6] G.R. Davies, T.K. Halstead, R.C. Greenhow, and K.J. Packer, *Chem. Phys. Lett.* **230**, 239 (1994); B.R. Patyal *et al.*, *J. Magn. Reson.* **126**, 58 (1997); M. Bock, *Magn. Reson. Med.* **38**, 890 (1997); D.M. Schmidt *et al.*, *J. Magn. Reson.* **129**, 184 (1997); H.U. Kauczor, R. Surkau, and T. Roberts, *Eur. Radiol.* **8**, 820 (1998), and references therein.  
 [7] C.H. Tseng, G.P. Wong, V.R. Pomeroy, R.W. Mair, D.P. Hin-

- ton, D. Hoffmann, R.E. Stoner, F.W. Hersman, D.G. Cory, and R.L. Walsworth, Phys. Rev. Lett. **81**, 3785 (1998).
- [8] R.W. Mair, D.G. Cory, S. Peled, C.H. Tseng, S. Patz, and R.L. Walsworth, J. Magn. Reson. A **35**, 478 (1998); R.W. Mair, G.P. Wong, D. Hoffmann, M.D. Hurlimann, S. Patz, L.M. Schwartz, and R.L. Walsworth, Phys. Rev. Lett. **83**, 3324 (1999).
- [9] T.E. Chupp, R.J. Hoare, R.L. Walsworth, and Bo Wu, Phys. Rev. Lett. **72**, 2363 (1994).
- [10] R.E. Stoner, M.A. Rosenberry, J.T. Wright, T.E. Chupp, E.R. Oteiza, and R.L. Walsworth, Phys. Rev. Lett. **77**, 3971 (1996).
- [11] D. Bear, T.E. Chupp, K. Cooper, S. DeDeo, M. Rosenberry, R.E. Stoner, and R.L. Walsworth, Phys. Rev. A **57**, 5006 (1998).
- [12] M.V. Romalis and W. Happer, Phys. Rev. A **60**, 1385 (1999).
- [13] T.G. Vold, F. Raab, B. Heckel, and E.N. Fortson, Phys. Rev. Lett. **52**, 2229 (1984).
- [14] T.E. Chupp, R.J. Hoare, R.A. Loveman, E.R. Oteiza, J.M. Richardson, M.E. Wagshul, and A.K. Thompson, Phys. Rev. Lett. **63**, 1541 (1989).
- [15] T.E. Chupp and R.J. Hoare, Phys. Rev. Lett. **64**, 2261 (1990).
- [16] D. Bear, R.E. Stoner, R.L. Walsworth, V.A. Kostelecky, and C.D. Lane, Phys. Rev. Lett. **85**, 5038 (2000).
- [17] M. Rosenberry and T.E. Chupp, Phys. Rev. Lett. **86**, 22 (2001).
- [18] V.A. Kostelecky and C.D. Lane, Phys. Rev. D **60**, 116010 (1999).
- [19] R.E. Stoner, in *CPT and Lorentz Symmetry*, edited by V.A. Kostelecky (World Scientific, Singapore, 1999), p. 201.
- [20] W. Happer, Rev. Mod. Phys. **44**, 169 (1972).
- [21] W. Happer and W.A. van Wijngaarden, Hyperfine Interact. **38**, 435 (1987).
- [22] S.R. Schaefer, G.D. Cates, T.R. Chien, D. Gonatas, W. Happer, and T.G. Walker, Phys. Rev. A **39**, 5613 (1989).
- [23] T.G. Walker, Phys. Rev. A **40**, 4959 (1989).
- [24] A. Ben-Amar Baranga, S. Appelt, M.V. Romalis, C.J. Erickson, A.R. Young, G.D. Cates, and W. Happer, Phys. Rev. Lett. **80**, 2801 (1998).
- [25] M.V. Romalis and G.D. Cates, Phys. Rev. A **58**, 3004 (1998).
- [26] T.E. Chupp (private communication).
- [27] M.E. Wagshul and T.E. Chupp, Phys. Rev. A **49**, 3854 (1988).
- [28] W. Zu, S.R. Schaefer, G.D. Cates, and W. Happer, Phys. Rev. A **37**, 1161 (1994).
- [29] C.B. Alcock, V.P. Itkin, and M.K. Horrigan, Can. Metall. Q. **23**, 309 (1984).
- [30] K. Hoffman and R. Kunze, *Linear Algebra* (Prentice-Hall, Englewood Cliffs, NJ, 1971), p. 280.
- [31] D.K. Walter, W.M. Griffith, and W. Happer, Phys. Rev. Lett. **86**, 3264 (2001).